Express Polymer Letters Vol.17, No.6 (2023) 610–624
Available online at www.expresspolymlett.com
https://doi.org/10.3144/expresspolymlett.2023.45

Research article

Rationally designed biomimetic bone scaffolds with hierarchical porous-architecture: Microstructure and mechanical performance

Vijay Shankar Kumawat[1,2], *Sanchita Bandyopadhyay-Ghosh*[1,2], *Subrata Bandhu Ghosh*[1,2*]

[1]Engineered Biomedical Materials Research and Innovation Centre, Manipal University Jaipur, 303007 Jaipur, India
[2]Department of Mechanical Engineering, Manipal University Jaipur, 303007 Jaipur, India

Received 19 October 2022; accepted in revised form 5 January 2023

Abstract. A biomimetic strategy was adopted by incorporating nano-fluorcanasite (nFC) within biocompatible and biodegradable poly-(ε-caprolactone) (PCL) matrix to obtain functionally tuned bio-nanocomposite bone scaffolds. A hybrid approach was adopted using fused deposition modelling, solvent casting and thermally induced phase separation to develop the scaffolds. Phase evolution study through X-ray diffraction revealed dominant crystalline phases (fluorcanasite and fluorapatite) and enhanced crystallinity of the scaffolds. Microstructural investigation through field emission-scanning electron microscopy revealed interconnected gradient porosities and hierarchical (meso, micro and macro) porous architecture within the scaffolds similar to natural bone. The elemental mapping study further confirmed higher calcium:phosphate (Ca:P) ratio upon nFC incorporation, desirable for bone repair. The volume visualisation through X-ray micro-computed tomography confirmed the presence of porous micro-architecture and homogenous dispersion of nFC particulates within the scaffolds. Mechanical performance of the bio-nanocomposite scaffolds was also found to be enhanced to sustain the load against pore collapse. Enhanced cell viability and cellular proliferation response with human osteosarcoma bone cells established the *in-vitro* biocompatibility of the scaffolds. Finally, this study opens up a unique pathway in the fabrication of biomimetic bone scaffolds with a highly conducive cellular environment.

Keywords: *biocomposites, bone scaffold, biomimetic, additive manufacturing, bone tissue engineering*

1. Introduction

Considering that natural bone contains inorganic nanostructured apatite bioceramic phase interdispersed within collagen biopolymer, a biomimetic composite bone scaffold aims to integrate nano-bioceramic reinforcement within biopolymer matrix to meet mechanical and physiological requirements of the host tissue [1]. In this regard, biopolymers (natural and synthetic) have demonstrated great potential towards simulating the extracellular matrix (ECM) and interacting with tissues. Natural biopolymers (collagen [2–4], gelatin [5, 6], chitosan [7, 8], cellulose [9, 10], alginate [11] *etc*.) have unique properties, such as low immunogenicity, ability to adsorb bioactive moieties, metabolic accessibility of degradation products, outstanding biodegradability and cytocompatibility. Unfortunately, these natural biopolymers have shown challenges, such as slow processing, batch-to-batch dissimilarity in their microstructure, and chemical heterogeneity, which further hinder their uses as bone scaffold biomaterial [12, 13]. Synthetic biopolymers (poly(lactic acid) [14], poly(ε-caprolactone) [15–17], poly(vinyl alcohol) [18, 19], poly(glycolic acid) [20, 21], poly(hydroxyalkanoate) [22, 23] *etc*.), on the other hand, are non-toxic, biodegradable, and amenable for modification with exceptional

*Corresponding author, e-mail: subratab.ghosh@jaipur.manipal.edu

blend-compatibility. Among them, poly(ε-caprolactone) (PCL), has already been established as a medically proven biopolymer, owing to its low melting temperature, high permeability in drug release and exceptional capability to withstand long-term tissue growth, making it a preferred choice for scaffold materials [24]. However, PCL lacks the required bioactivity to regenerate and augment the fractured bones. Osteoconductive bioceramics (hydroxyapatite [25], beta-tricalcium phosphate [26], *etc*.) and bioglasses (silicate-; phosphate-; borate-based) in this regard, has gained popularity owing to their excellent biocompatibility and bioactivity, although, their inherent brittleness and insufficient mechanical performance (low compressive strength and fracture toughness), limit their use as bone scaffold [1, 13]. To this end, a possible approach is to develop osteoconductive glass-ceramics by converting amorphous bioglasses into tough and polycrystalline glass-ceramics through controlled crystallisation process. Modified fluorcanasite, a chain-silicate glass-ceramic, has shown high potential owing to its bulk nucleating nature and interpenetrating needle-like microstructure, resulting into high mechanical performance (flexural strength and fracture toughness), thereby making it a suitable candidate as bone scaffold [27–33]. Apart from materials, the selection of appropriate scaffold fabrication technique is also critically important. Thermally-induced phase separation (TIPS), in this regard, has generated notable attention due to its efficacy in simulating porous nano-architecture of natural bone and the ability to integrate bioactive molecules [34]. Unfortunately, this technique is inadequate to reproduce well-defined porous structure within bone scaffolds [35, 36]. In contrast, fused deposition modelling (FDM), an additive manufacturing (AM) technique, holds promise to produce scaffolds with delicate features such as design customisation, structural reproducibility, quick processing and low cost [37]. However, FDM technique has some inherent limitations in terms of incorporation of nanofillers within the polymer matrix and generation of ultrafine porosity (<2 μm), restricting its widespread use in composite scaffold fabrication [38, 39]. Against this background, we report a biomimetic route of incorporating nano-fluorcanasite (nFC) in PCL biopolymer matrix towards developing bio-nanocomposite bone scaffolds. We adopted a unique hybrid approach by combining FDM, solvent casting and TIPS to obtain new directives in the fabrication of porous bone scaffolds with integrated meso, micro and macro pores.

2. Fabrication of bio-nanocomposite scaffolds

To fabricate the biomimetic composite scaffold, nano-fluorcanasite particulates (nFC) were synthesised following a previously reported method [40]. Further, FDM based three-dimensional (3D) printer (Ultimaker 3, Netherlands) was employed to fabricate fugitive moulds of poly(vinyl alcohol) (PVA) with interconnected macro pores. Temperature-controlled nozzle moving in the *x*–*y* plane and *z*-direction was used to build layer-by-layer 3D construction of the desired shape, as shown in Figures 1a and 1b. Finally, a novel hybrid approach involving FDM, solvent casting and TIPS was used to fabricate a range of scaffolds. In this technique, as prepared nFC suspension in chloroform was propelled into neat PCL solution (in chloroform), followed by probe-sonication (VCX 750, Vibra cell, USA) for 20 min at 60% amplitude to facilitate efficient dispersion of nFC (step-1, Figure 1c). Prepared neat PCL and nFC/PCL suspension were solvent cast into PVA mould, placed in a retractable Teflon chamber (step-2, Figure 1c). Solidification of neat PCL and bio-nanocomposite suspensions was achieved through the TIPS technique, by immersing the Teflon chamber into liquid nitrogen for 10 min, followed by freeze-drying in lyophiliser (Grace Instruments, India) at –40 °C for 3 days to remove residual solvent and air-bubbles (step-3, Figure 1c). Furthermore, all specimens were soaked in deionised water for 3 days to leach out fugitive PVA mould (step-4, Figure 1c). Finally, developed scaffolds were sterilised, vacuum dried and stored in a desiccator.

3. Characterisations

Nano-fluorcanasite particulates, PVA mould, neat PCL scaffold and bio-nanocomposite scaffolds with nFC loading of 20, 30 and 50 wt%, respectively, were investigated using various characterisation techniques. X-ray diffraction (XRD) studies were performed using D500 X-ray diffractometer (Siemens, Germany), where the samples were held in aluminium holder and irradiated with Cu-radiation (λ = 1.5406 Å) between the angle interval of 5° 2θ to 70° 2θ with a scan speed of 2° 2θ min^{-1}. Field emission-scanning electron microscopy (FE-SEM, JSM-7610FPlus, Jeol, Japan) was used to investigate

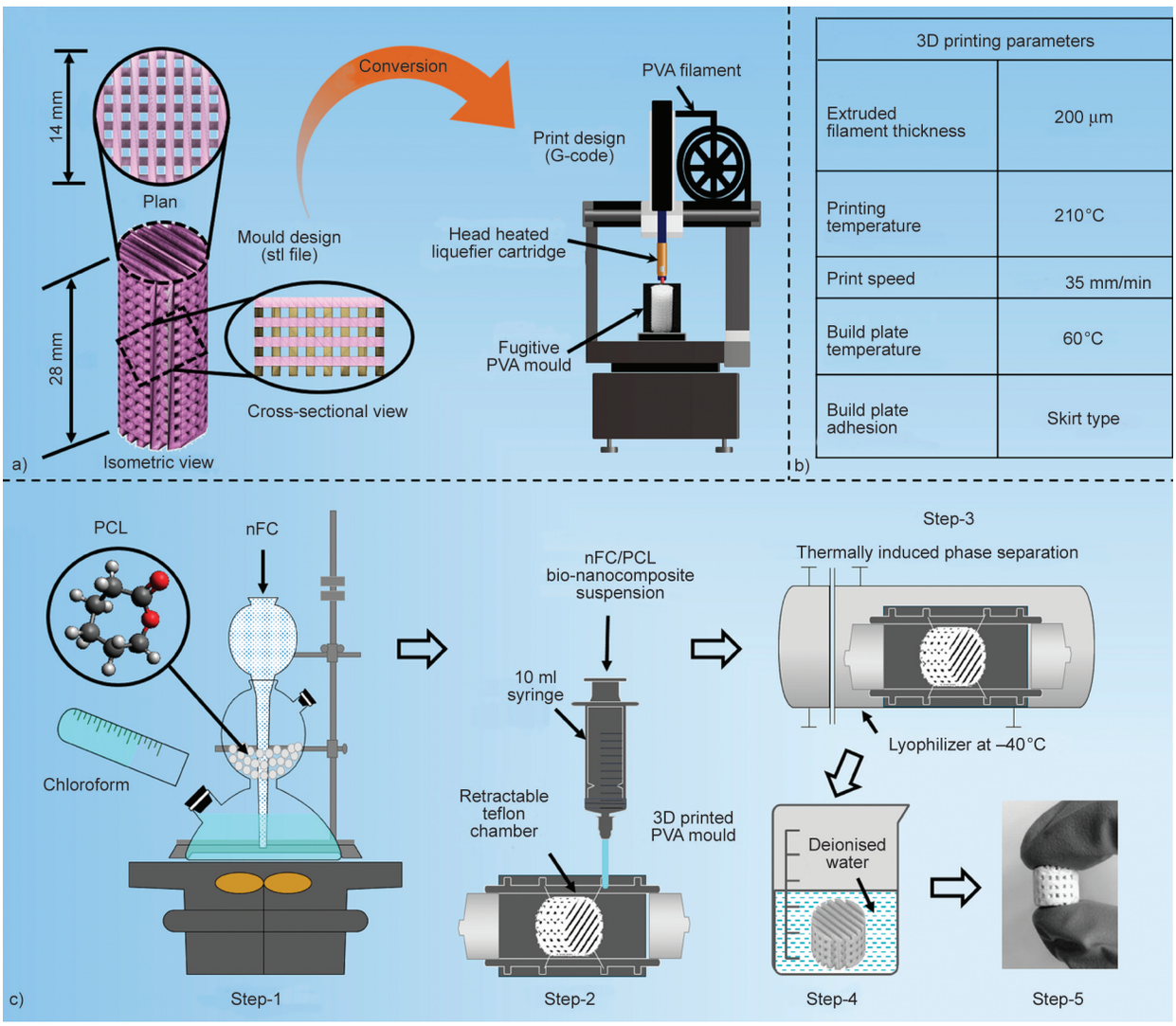

Figure 1. a) Fabrication process of 3D printed PVA mould; 1: Computer-aided design of PVA mould exhibiting square mesh geometry through cross-sectional and top view (plan); 2: schematic representation of FDM 3D printing of PVA mould; b) 3D printing parameters; c) development of porous bio-nanocomposite scaffolds using hybrid approach; step-1: preparation of nFC/PCL bio-nanocomposite suspension; step-2: solvent casting of nFC/PCL suspension into PVA mould; step-3: TIPS technique to generate gradient porosity; step-4: aqueous dissolution of fugitive PVA mould; step-5: vacuum dried scaffolds.

microstructural features. For this, initially, all the samples were vacuum dried and coated with gold-palladium (Au-Pd) using a sputter coater (Jeol, USA) to avoid electrostatic charging. Energy dispersive spectroscopy (EDS by EDAX, Ametek, USA) was carried out to understand the elemental compositions of the Au-Pd coated samples. X-ray micro-computed tomography (Indus-2 synchrotron imaging beamline, BL-4, RRCAT Indore, India) operated at 2.5 GeV at 300 mA was employed, and the image slices were subjected to 3D volume rendering using Fiji ImageJ software to observe the particle distribution and micro-architecture of developed scaffolds. The mechanical performances of all the developed scaffolds with square mesh were characterised by compression test on a universal testing machine (DAK systems, 9202, India) using a 10 kN load cell. *In-vitro* cell culture experiments were performed to evaluate the viability of human osteosarcoma (MG-63) cells on developed scaffolds and control samples. The cells were grown at 37 °C (5% CO_2 and 95% relative humidity) in Dulbecco's modified eagle medium (DMEM) and supplemented with 15% fetal bovine serum (FBS) and 1% antibiotics, following which they were seeded (10^4 cells/ml) into 24 well plates, incubated and permeabilised. The cytoskeleton and nucleus of MG-63 cells were then stained with Alexa Fluor™ 488 Phalloidin (green) and DAPI (blue) dyes, respectively. Finally, the cell-seeded scaffold samples were observed under a fluorescence microscope

(Nikon Eclipse LV 100 ND) to examine their cell viability.

4. Results and discussion

4.1. X-ray diffraction

Crystalline phase evolution was identified through XRD traces of PVA mould, neat PCL scaffold, nFC glass-ceramic particulates and bio-nanocomposite scaffolds with nFC loading of 20, 30 and 50 wt%, respectively, as shown in Figure 2. The XRD spectrum of PVA mould recorded a semi-crystalline hump at 19.8° 2θ, corresponding to the (101) lattice orientation (JCPDS card no: 00-058-0991$^{(O)}$) [41]. XRD trace of neat PCL scaffold fabricated through aqueous dissolution of PVA mould also depicts semi-crystalline nature, with two sharp diffraction peaks of ε-caprolactone phase of the orthorhombic crystal structure at Bragg angles 21.36° 2θ and 23.67° 2θ corresponding to the (110) and (200) lattice orientations respectively [42–44]. These sharp diffraction peaks originate due to intramolecular interactions between ordered PCL chains through their hydrogen bonding [45]. Figure 2 also shows the XRD trace of nFC glass-ceramic, revealing its polycrystalline nature with crystalline phases, including frankamenite (JCPDS card no: 00-045-1398$^{(I)}$; 01-087-1149$^{(I)}$) (also referred to as canasite-A) and fluorcanasite (JCPDS card no: 01-072-8231$^{(*)}$; 00-013-0553$^{(B)}$) as primary crystalline phases with overlapping peaks at 28.91° 2θ and 30.65° 2θ, corresponding to (600), (300) and (022), ($\bar{1}$22) lattice orientations, respectively [46]. Other crystalline phases that could be

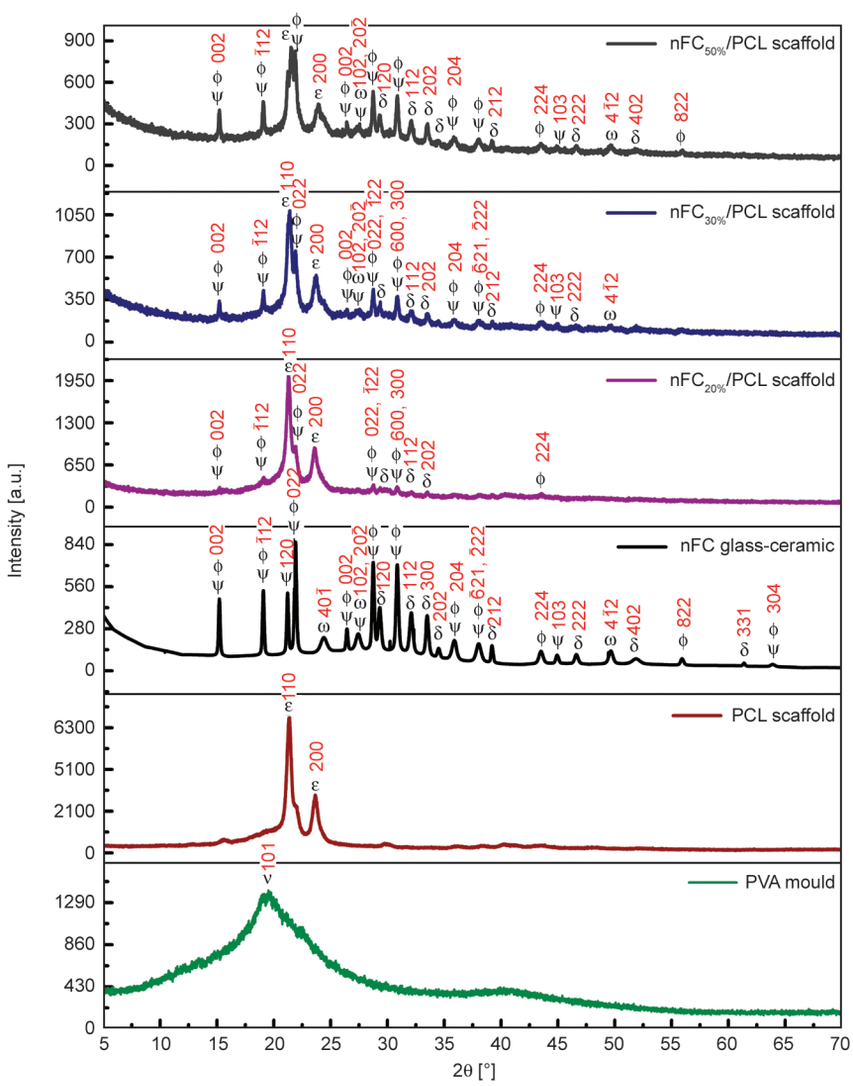

Figure 2. XRD spectra of PVA mould, neat PCL scaffold, nFC particulates and bio-nanocomposite scaffolds showing respective crystalline phases of PVA (v), poly(ε-caprolactone) (ε), fluorcanasite (ϕ), frankamenite (ψ), fluorapatite (δ), xonotlite (ω).

identified were fluorapatite (JCPDS card no: 00-076-0558$^{(I)}$; 01-073-9695$^{(I)}$; 00-021-0145$^{(I)}$) with highest peaks at 32.05° 2θ, 32.21° 2θ and 33.27° 2θ, corresponding to (211), (112) and (300) lattice orientations respectively [47–49] and xonotlite (JCPDS card no: 01-074-3008/3009/3010$^{(H)}$) with their highest crystalline peaks at 24.37° 2θ, 27.43° 2θ and 49.52° 2θ, corresponding to (40$\bar{1}$), ($\bar{2}$02) and (4$\bar{1}$2) lattice orientations, respectively [48, 50]. Figure 2 also illustrates that the incorporation of nano-particulates of FC glass-ceramic, used as reinforcement in bio-nanocomposite scaffolds, resulted in the emergence of additional crystalline peaks from nFC and declination of the characteristic peak intensity of ε-caprolactone phase of PCL, which could be attributed to the fact that increased loading nFC, resulted in decreased orientation and in disruption of the ordering of PCL chains within the crystalline domain.

Additionally, the absence of new peaks, apart from PCL and nFC glass-ceramics, indicated complete aqueous dissolution of PVA mould. The overall % degree of crystallinity of PCL scaffolds and bio-nanocomposite scaffolds was determined using Equation (1):

$$\text{Crystallinity, } X_c\,[\%] = \frac{\sum A_{cryt}}{\sum A_{cryt} + \sum A_{amp}} \cdot 100 \quad (1)$$

where, $\sum A_{cryt}$ is the sum of areas of crystalline phases and $\sum A_{amp}$ is the sum of areas of amorphous profiles. Percentage crystallinity of the PCL scaffold was found to be 44.8%, while overall percentage crystallinities of bio-nanocomposite scaffolds were found to be enhanced by the incorporation of nFC particulates. Percentage crystallinity of bio-nanocomposite with 20, 30 and 50 wt% loading of nFC had a crystallinity of 50.4, 57.2 and 61.3%, respectively. The increase in overall crystallinity could be attributed to the heterogeneous nucleation effect (leading to the formation of more but smaller PCL crystals) and homogeneous distribution of nFC within PCL chains in addition to the coexistence of various crystalline phases within nFC, resulting in efficient packing of crystal planes within the bio-nanocomposites scaffolds [51]. The XRD results, therefore, signify efficient integration and promising potential of nFC as reinforcement.

4.2. Field emission-scanning electron microscopy

The microstructural investigation (Figure 3a) of synthesised nFC and scaffolds revealed several interesting features. Figure 3a$_1$ shows photomicrographs synthesised nFC particulates, while Figure 3a$_2$ shows FE-SEM micrograph of nFC confirming that the particulates were brought down to nanoscale. Figure 3a$_3$ depicts the elemental mapping of nFC through energy dispersive spectroscopy (EDS). As anticipated, silicon (Si) recorded the highest intensity amongst the characteristic peaks of the constituent elements (Si, Ca, P, Na, K). The absence of other elements confirmed minimal contamination during the synthesis process. Figure 3b shows a photograph of a developed neat PCL scaffold and nFC$_{x\%}$/PCL scaffolds showing gradual reduction in transparency with increasing nFC content within PCL matrix. Figure 3c shows the FE-SEM micrographs of PVA mould (Figure 3c$_1$), neat PCL (Figure 3c$_2$), nFC$_{20\%}$/PCL (Figure 3c$_3$), and nFC$_{30\%}$/PCL (Figure 3c$_4$), and nFC$_{50\%}$/PCL (Figure 3c$_5$) scaffolds. Figure 3c$_1$ shows the surface topology of the PVA mould. Superimposition of PVA layers could be observed, indicating successful generation of micro-channels of defined dimensions. Figure 3c$_2$–3c$_5$) reveals the layered microstructure of developed scaffolds, originating from the negative impression of PVA mould walls, signifying the complete dissolution of fugitive PVA mould and indicating a favourable porous environment including macroporous channels (~1000 μm) and interconnected pore network for sufficient transportation of minerals and nutrients to defective bone sites.

Figure 4 shows FE-SEM micrographs of cross-sectional threads at 1000×, 20 000× and 40 000× magnifications and EDS spectra of developed scaffolds. Figures 4a$_1$, 4b$_1$, 4c$_1$, 4d$_1$ demonstrate the formation of internal micropores within the scaffolds. Figures 4a$_2$, 4b$_2$, 4c$_2$, 4d$_2$ reveal the presence of micropores (up to 2 μm) with interconnected microstructure, which could otherwise be difficult to achieve through FDM alone. It is important to note that such a hierarchical porous environment in the scaffold is highly favourable for the transport of nutrients and filtration of wastes which in turn is anticipated to bring benefits for cell proliferation and cell adhesion to promote bone formation [52]. Figures 4a$_3$, 4b$_3$, 4c$_3$, 4d$_3$ revealed the presence of unique zones with mesoporous (20–50 nm) networks, which are anticipated to bring benefits in terms of cell seeding and flirtation of waste nutrients. It could also be observed that higher loading of nFC, resulted in a more apparent cellular network structure, possibly owing to the nucleating effect of nFC. The cellular

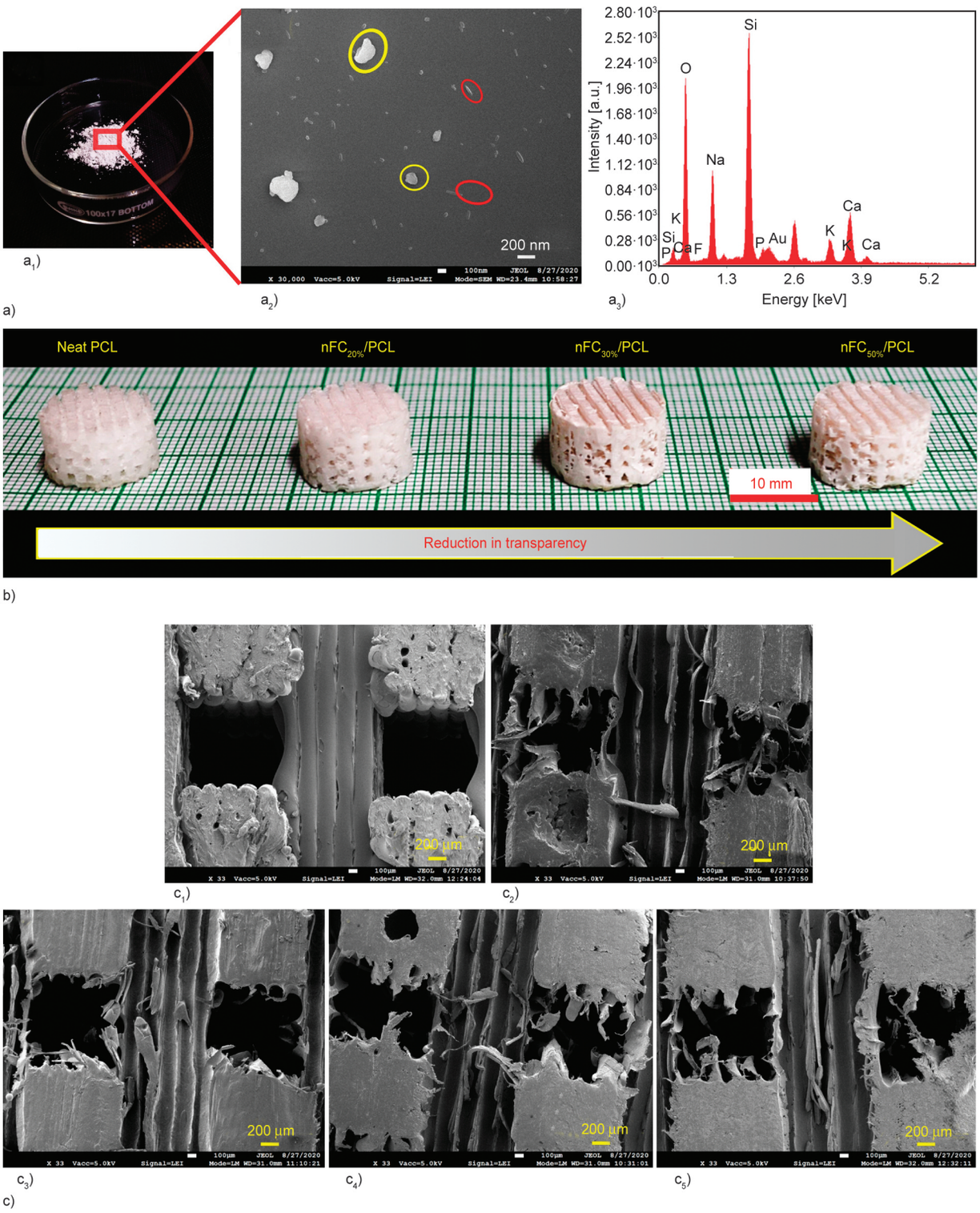

Figure 3. a) Photomicrograph of: a_1) nFC particulates; a_2) FE-SEM image of nFC showing individualised (red circle) and few aggregated particles (yellow circle); a_3) elemental analysis of nFC particulates through EDS. b) Photographs of developed scaffolds showing gradual reduction in transparency with increasing nFC content within PCL matrix. c) FE-SEM micrographs of: c_1) external lateral surfaces of PVA mould; c_2)–c_5) scaffolds showing layered microstructure originated from negative impression of PVA mould wall.

environment integrated with meso, micro and macro pores, therefore, demonstrates the efficiency of using the hybrid approach to develop biomimetic bone scaffold.

Figure 5 show elemental mapping, where the scaffolds recorded presence of characteristic peaks of all constituent elements from nFC and PCL. It is evident from the results that with increased loading of nFC,

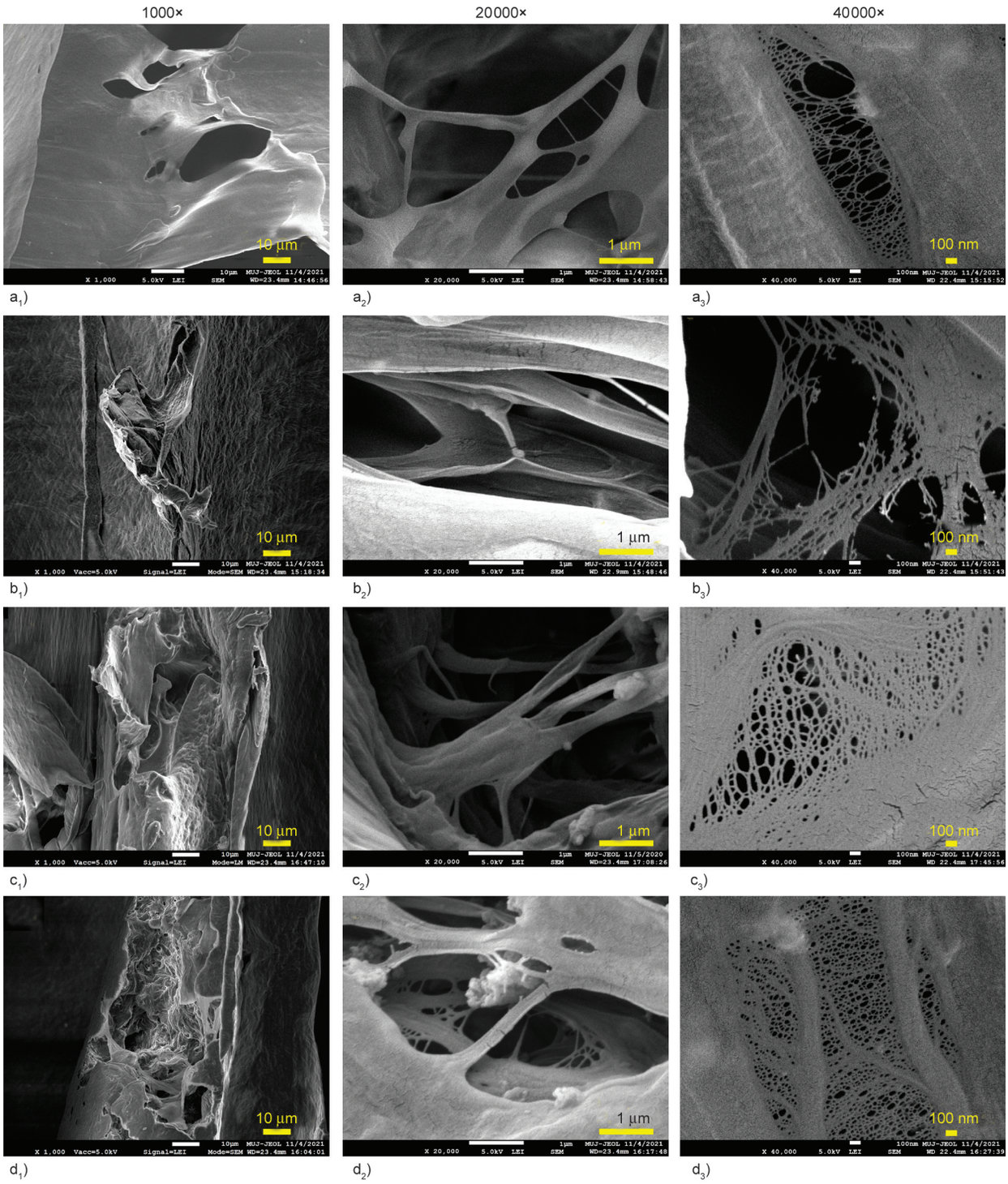

Figure 4. FE-SEM micrographs of cross-sectional threads of scaffolds at 1000×, 20 000× and 40 000×: a_1)–a_3) neat PCL; b_1)–b_3) $nFC_{20\%}$/PCL; c_1)–c_3) $nFC_{30\%}$/PCL; d_1)–d_3) $nFC_{50\%}$/PCL.

intensities of characteristic elements of PCL were marginally reduced, while that of nFC were gradually increased, shifting towards a higher Ca:P ratio, a feature desirable for bone repair [53].

4.3. X-ray micro-computed tomography

Reconstructed volumetric 3D micro-architecture of the $nFC_{x\%}$/PCL (where, x = 0, 20, 30 and 50%) scaffolds are shown in Figures 6a_1, 6b_1, 6c_1, 6d_1). The 3D rendering of the micro-tomographic images of 2D slices demonstrated a porous micro-architectural environment, which established the efficacy of the hybrid approach used in scaffold fabrication to generate biomimetic bone architecture. It can also be observed that with increased loading of nFC particulates, the bio-nanocomposite bone scaffolds acquired

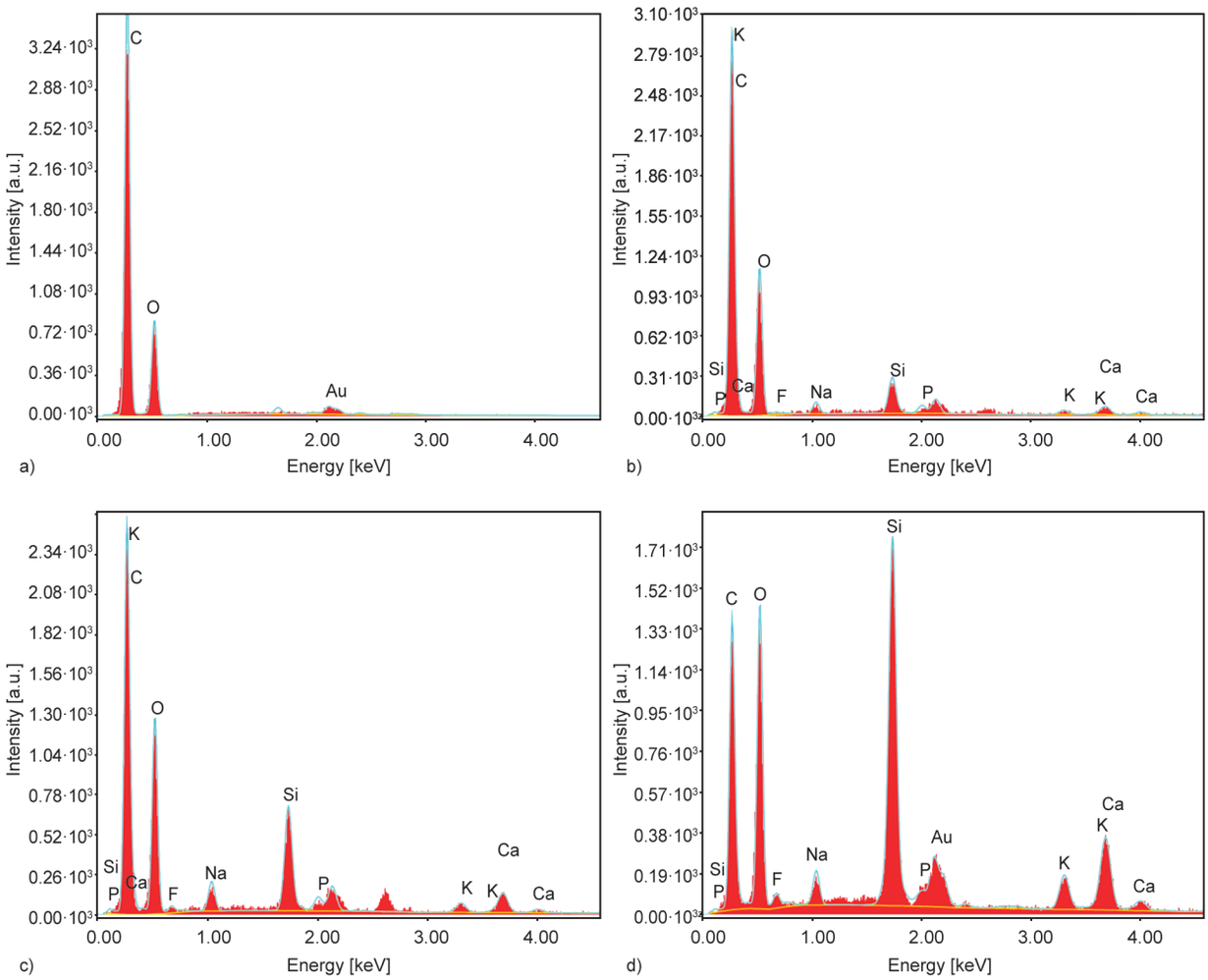

Figure 5. EDS spectra through elemental analysis: a) neat PCL; b) $nFC_{20\%}$/PCL; c) $nFC_{30\%}$/PCL; d) $nFC_{50\%}$/PCL.

more precisely defined boundaries, resulting in uniform pore architecture and in turn, increased structural integrity of the scaffold. Figures $6a_2$, $6b_2$, $6c_2$, $6d_2$), on the other hand, show the distribution of nanoparticulates in the 3D micro-architecture of developed scaffolds. It can be observed that the architecture of the neat PCL scaffold (Figure $6a_2$) shows the polymer struts only during the threshold process, owing to the absence of nFC particulates. While Figures $6b_2$, $6c_2$, $6d_2$ show the uniform distribution of nano-particulates with minimal agglomeration at square mesh channels of composite threads with minimal evidence of particle agglomeration at higher loadings. The biomimetic 3D porous micro-architecture of the developed scaffolds revealed by x-ray micro-CT is in good agreement with the FE-SEM results and provides conducive environment for bone tissue growth.

4.4. Mechanical properties

Mechanical performances of developed scaffolds were evaluated under monotonic unconstrained compression load as per ASTM standard (D695-15). Figure 7a shows that all scaffolds demonstrated similar fracture behaviour, namely, an initial elastic response followed by a considerable plastic deformation before fracture, a typical characteristic of highly porous polymers. All scaffolds could sustain load up to 40% strain, and with the increase in nFC loading, both initial modulus and maximum stress values increased, with an accompanying reduction in elongation values. Ultimate compressive strengths of scaffolds were found to be influenced by the incorporation of nFC with strength values of 6.2±0.3 MPa, 7.1±0.6 MPa (↑14.5%), 7.8±0.3 MPa (↑25.80%) and 8.8±0.4 MPa (↑41.93%) respectively for 0, 20, 30 and 50 wt% nFC loading, indicating the significant reinforcing potential of nFC within PCL matrix. Figure 7b shows the compressive modulus of scaffold specimens calculated through the elastic region of the stress-strain curves. The modulus values were found to be 47.9±4.8, 75.7±6.9, 87±4.1 and 90.6±5.8 MPa for scaffold specimens with 0, 20, 30 and 50 wt%

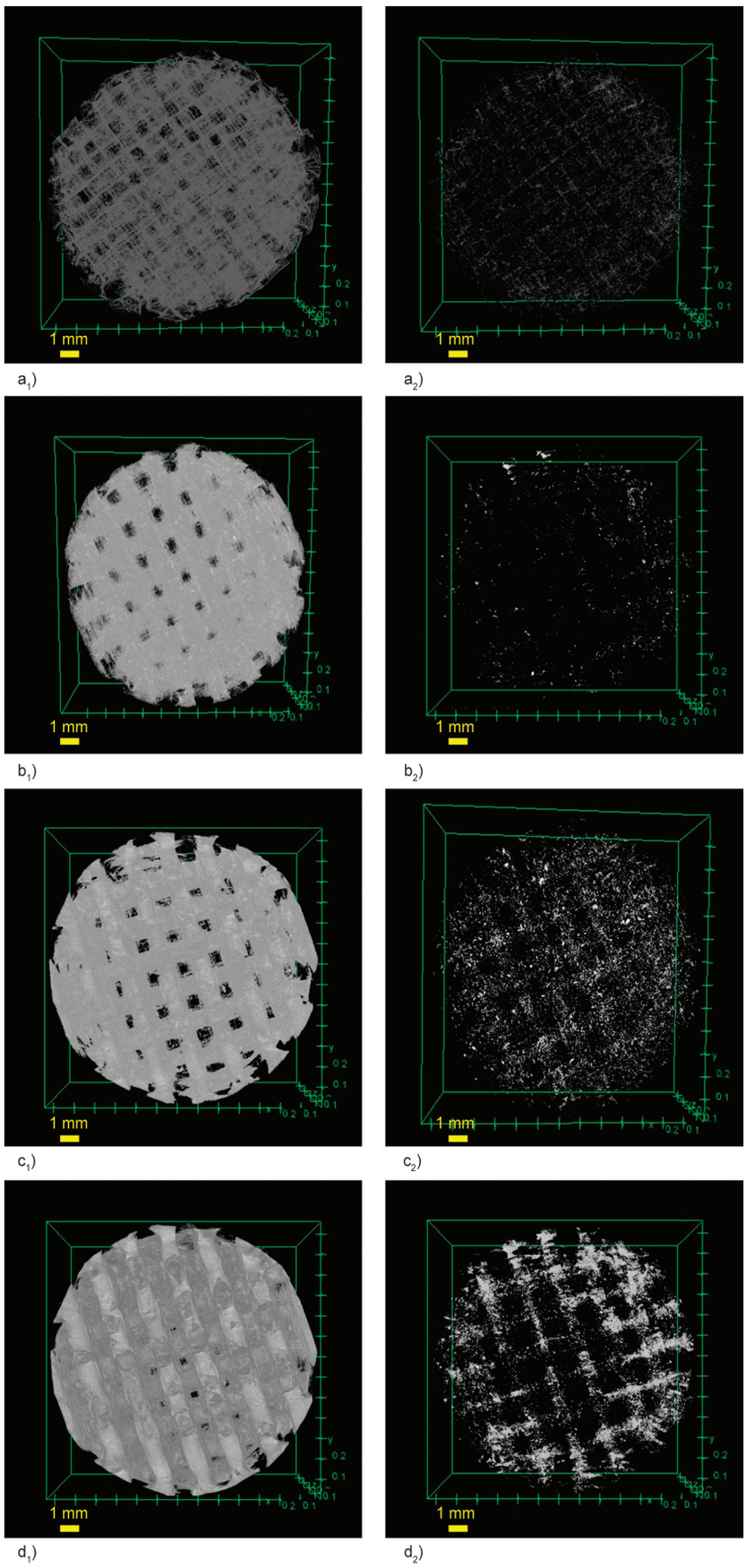

Figure 6. X-ray micro-CT images, showing volumetric 3D micro-architecture of: a_1) and a_2) neat PCL; b_1) and b_2) $nFC_{20\%}$/PCL; c_1) and c_2) $nFC_{30\%}$/PCL; d_1) and d_2) $nFC_{50\%}$/PCL scaffold samples show porous micro-environment and distribution of nFC particulates within the bio-nanocomposite scaffolds.

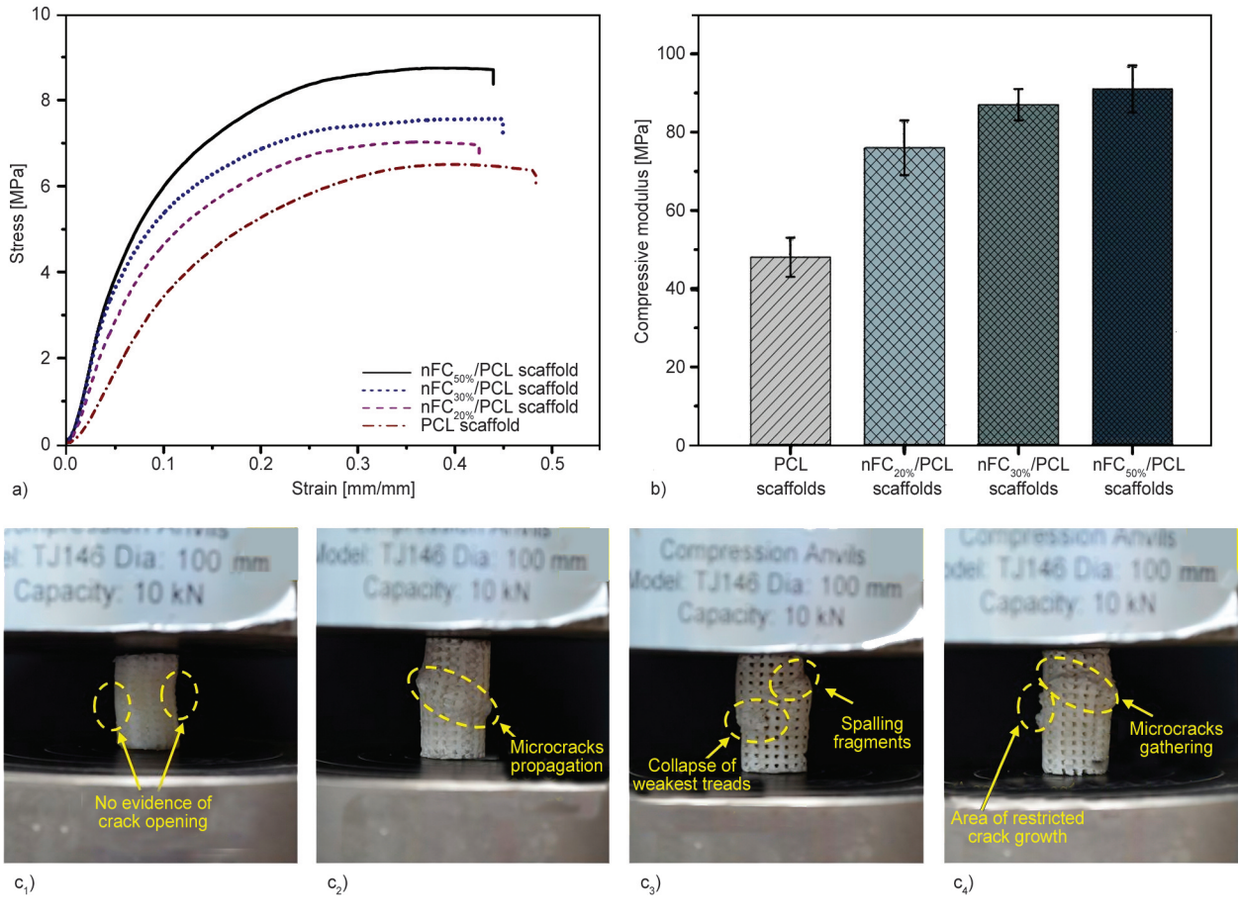

Figure 7. Mechanical performance of $nFC_{x\%}$/PCL scaffold specimens (where x = 0, 20, 30 and 50%) under monotonic unconstrained compression load showing a) stress-strain curves; b) compressive modulus; c_1)–c_4) pore collapse behaviour.

nFC loading respectively. The results could be attributed to the reinforcing effect of the nFC, with nFC particulates acting as potential barriers to crack opening. This is also an indication that nFC particulates were efficiently dispersed within the PCL matrix. The higher elongation of neat PCL scaffold also stems from the unrestricted mobility of polymeric chains, which was not the case with bio-nanocomposite scaffolds. The reinforcing potential of nFC was found to be higher than the reported values of conventional nano-hydroxyapatite (nHA) used as fillers within PCL matrix at similar loading levels [54–58]. The results are also in line with our XRD results (Figure 2), where increased loading of nFC resulted in increased crystallinity of the bio-nanocomposite scaffolds and in turn, the enhancement of rigidities of the scaffold samples. It is interesting to note that with increased loading of nFC, compressive strength and modulus values of the scaffolds could encompass the entire range of load-bearing capacity of cancellous bone and lower range of cortical bone [54, 59, 60].

Figures $7c_1$–$7c_4$ show fractured cylindrical scaffold specimens. While PCL scaffold did not demonstrate any evidence of failure in crack propagation, the bio-nanocomposite scaffolds showed evidence of clear crack propagation. This can be attributed to the fact that neat PCL scaffold being less rigid, typical crack growth behaviour of brittle specimens could not be observed, whereas, with increased incorporation of nFC, the samples became more rigid and brittle crack propagations were more evident. It is also important to note that fractured bio-nanocomposite scaffold specimens demonstrated multiple cracks, owing to the collapse of the weakest threads, instead of a single large crack, thereby confirming the role of nFC in restricting crack growth. Overall, the tunable mechanical strength with varying loading of nFC is highly desirable to match the mechanical properties of the surrounding bone tissues and to avoid the stress-shielding effect at the implantation site.

4.5. *In-vitro* biocompatibility

In-vitro cellular responses of human osteosarcoma (MG-63) bone cells on the scaffold samples were investigated through fluorescence microscopy imaging technique by using Alexa Fluor™ 488 Phalloidin

F-actin green fluorescence (for cytoskeleton) and DAPI blue fluorescence (for cell nuclei) following three days of post-seeding. As shown in Figure 8, all bio-nanocomposite scaffold samples demonstrated increased biomimetic and cell adhesion responses as compared to control and neat scaffold samples. It was observed that with increased loading of nFC particulates, enhanced cell lamellipodia and filopodia extensions were evident, indicating accelerated cell proliferation response and growth. At the highest nFC loading level (50 wt%), the cultured MG-63 cells were densely populated, exhibiting a higher degree of spreading with multiple nuclei surrounded by mature cytoskeleton. The cell viability results clearly indicated *in-vitro* biocompatibility of the bio-nanocomposite scaffolds, thereby establishing their potential in bone tissue engineering applications.

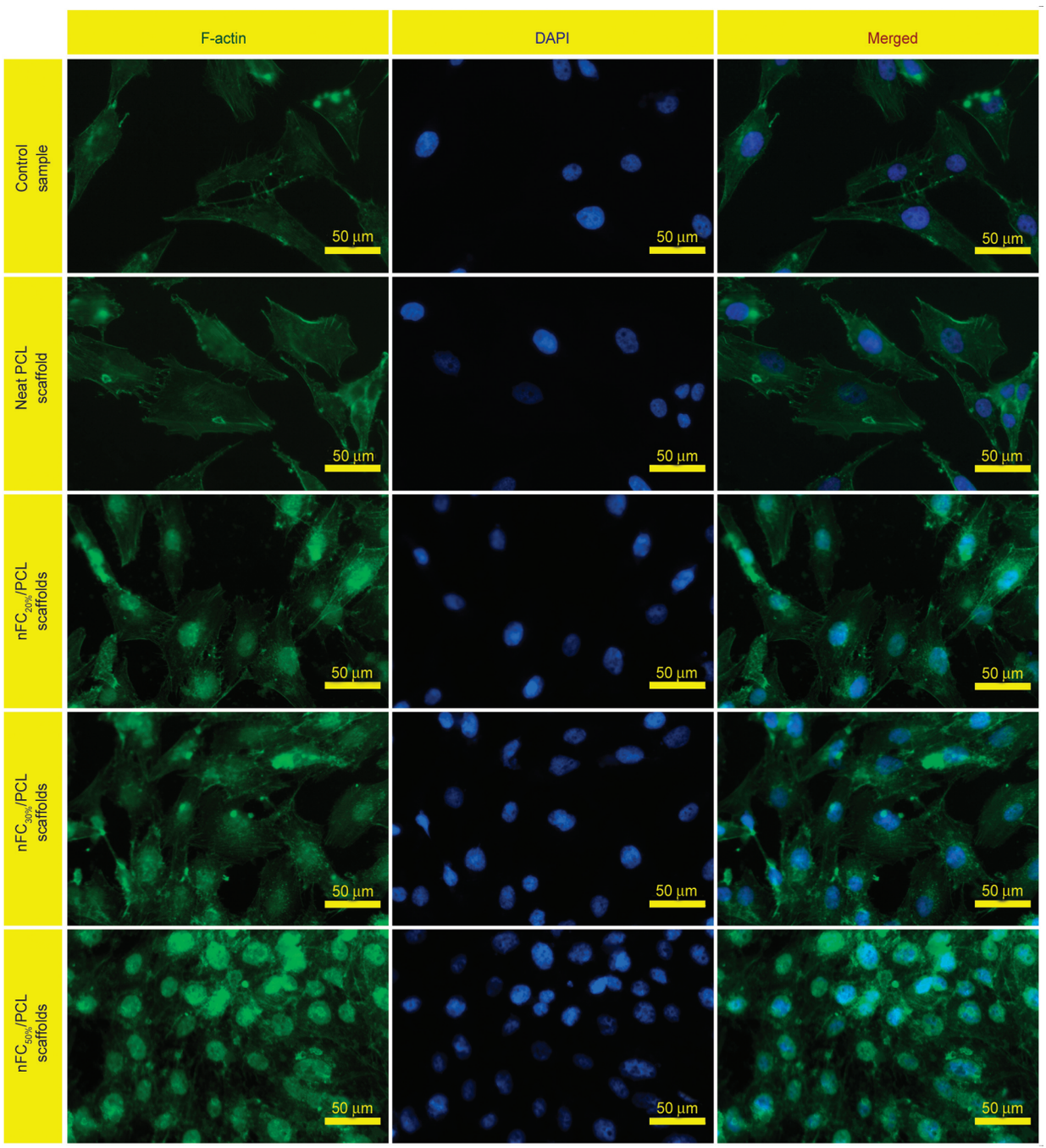

Figure 8. Fluorescence microscopic images of cytoskeleton (dyed with green F-actin), cell nuclei (dyed with blue DAPI), and merged (cytoskeleton and cell nuclei) of human osteosarcoma (MG-63) bone cells, showing cell adhesion and growth on control, neat PCL scaffold, and $nFC_{x\%}$/PCL bio-nanocomposite scaffolds with nFC loading (where x = 20, 30, and 50%) respectively.

5. Conclusions

Biomimetic composite scaffolds were developed with nFC reinforcement integrated within the PCL matrix for their anticipated use as bone substitute biomaterials. Crystalline phase evolution of the scaffolds with varying loading of nFC revealed the presence of characteristic crystalline peaks of PCL and that of nFC with dominant polycrystalline phases, such as fluorcanasite, frankamenite, and fluorapatite. The nanocomposite scaffolds exhibited an enhanced degree of crystallinity, which could be attributed to the heterogeneous nucleation effect of nFC particulates. Microstructural studies through FE-SEM further revealed favourable cellular environment with gradient porosities containing meso, micro and macro pores within the developed scaffolds, a prerequisite for ideal tissue-engineering scaffolds. This hierarchical porous architecture was achieved through a unique hybrid approach, thereby facilitating cell attachment and cell adhesion to promote bone formation. The porous micro-structural details were further supported by X-ray micro-CT investigation. The reconstructed 3D micro-architecture also revealed uniform distribution of nFC with minimal particle agglomeration at higher loadings. Ultimate compressive strength and compressive modulus of the bio-nanocomposite scaffolds under monotonic unconstrained loading increased with increased nFC loading and were found to be in the range of 7.1 to 8.8 MPa and between 75.7 to 90.6 MPa respectively, which falls within the entire load carrying capacity of cancellous bone. The *in-vitro* biocompatibility of the bio-nanocomposite scaffolds was confirmed by the cell viability and cellular proliferation response of human osteosarcoma (MG-63) bone cells. Overall, this study establishes a unique hybrid approach towards developing high-performance bio-nanocomposite bone scaffold.

Acknowledgements

The authors acknowledge Science and Engineering Research Board-Department of Science and Technology (SERB-DST), New Delhi, India, for providing 'Research Grant' [EMR/2016/007981] and Manipal University Jaipur, India, for providing 'Seed Grant' [MUJ/REGR/1435/05] for supporting this research. The authors also acknowledge Raja Ramanna Centre for Advanced Technology (RRCAT), Indore, Indian Institute of Technology-BHU, Varanasi, and Sophisticated Analytical Instrument Facility (SAIF), Manipal University Jaipur for providing the necessary characterisation facilities.

References

[1] Montazerian M., Zanotto E. D.: History and trends of bioactive glass-ceramics. Journal of Biomedical Materials Research Part A, **104**, 1231–1249 (2016). https://doi.org/10.1002/jbm.a.35639

[2] Cunha F. B., Pomini K. T., de Guzzi Plepis A. M., da Conceição Amaro Martins V., Machado E. G., de Moraes R., de Azevedo e Souza Munhoz M., Machado M. V. R., Duarte M. A. H., Alcalde M. P., Buchaim D. V., Buchaim R. L., Fernandes V. A. R., de Souza Bastos Mazuqueli Pereira E., Pelegrine A. A., da Cunha M. R.: *In vivo* biological behavior of polymer scaffolds of natural origin in the bone repair process. Molecules, **26**, 1598 (2021). https://doi.org/10.3390/molecules26061598

[3] Koo Y., Lee H., Lim C. S., Kwon S. Y., Han I., Kim G. H.: Highly porous multiple-cell-laden collagen/hydroxyapatite scaffolds for bone tissue engineering. International Journal of Biological Macromolecules, **222**, 1264–1276 (2022). https://doi.org/10.1016/j.ijbiomac.2022.09.249

[4] Fraile-Martínez O., García-Montero C., Coca A., Álvarez-Mon M. A., Monserrat J., Gómez-Lahoz A. M., Coca S., Álvarez-Mon M., Monserrat J., Gómez-Lahoz A. M., Coca S., Álvarez-Mon M., Acero J., Bujan J., García-Honduvilla N., Asúnsolo Á., Ortega M. A.: Applications of polymeric composites in bone tissue engineering and jawbone regeneration. Polymers, **13**, 3429 (2021). https://doi.org/10.3390/polym13193429

[5] Liu X., Ma P. X.: Phase separation, pore structure, and properties of nanofibrous gelatin scaffolds. Biomaterials, **30**, 4094–4103 (2009). https://doi.org/10.1016/j.biomaterials.2009.04.024

[6] Nagarajan S., Belaid H., Radhakrishnan S., Teyssier C., Balme S., Miele P., Cornu D., Subbaraya N. K., Cavaillès V., Bechelany M.: Sacrificial mold-assisted 3D printing of stable biocompatible gelatin scaffolds. Bioprinting, **22**, e00140 (2021). https://doi.org/10.1016/j.bprint.2021.e00140

[7] Gan D., Liu M., Xu T., Wang K., Tan H., Lu X.: Chitosan/biphasic calcium phosphate scaffolds functionalized with BMP-2-encapsulated nanoparticles and RGD for bone regeneration. Journal of Biomedical Materials Research Part A, **106**, 2613–2624 (2018). https://doi.org/10.1002/jbm.a.36453

[8] Liu G., Sun J., Gong M., Xing F., Wu S., Xiang Z.: Urine-derived stem cells loaded onto a chitosan-optimized biphasic calcium-phosphate scaffold for repairing large segmental bone defects in rabbits. Journal of Biomedical Materials Research Part B, **109**, 2014–2029 (2021). https://doi.org/10.1002/jbm.b.34850

[9] Kim M., Yeo M., Kim M., Kim G.: Biomimetic cellulose/calcium-deficient-hydroxyapatite composite scaffolds fabricated using an electric field for bone tissue engineering. RSC Advances, **8**, 20637–20647 (2018). https://doi.org/10.1039/c8ra03657h

[10] Phogat K., Kanwar S., Nayak D., Mathur N., Ghosh S. B., Bandyopadhyay-Ghosh S.: Nano-enabled poly(vinyl alcohol) based injectable bio-nanocomposite hydrogel scaffolds. Journal of Applied Polymer Science, **137**, 48789 (2020). https://doi.org/10.1002/app.48789

[11] Kumar A., Wang X., Nune K. C., Misra R. D. K.: Biodegradable hydrogel-based biomaterials with high absorbent properties for non-adherent wound dressing. International Wound Journal, **14**, 1076–1087 (2017). https://doi.org/10.1111/iwj.12762

[12] Reddy M. S. B., Ponnamma D., Choudhary R., Sadasivuni K. K.: A comparative review of natural and synthetic biopolymer composite scaffolds. Polymers, **13**, 1105 (2021). https://doi.org/10.3390/polym13071105

[13] Kumawat V. S., Bandyopadhyay-Ghosh S., Ghosh S. B.: An overview of translational research in bone graft biomaterials. Journal of Biomaterials Science, Polymer Edition, **34**, 497–540 (2022). https://doi.org/10.1080/09205063.2022.2127143

[14] Deng X., Liu Y., Yuan M., Li X., Liu L., Jia W. X.: Preparation and characterization of poly-DL-lactide-poly(ethylene glycol) microspheres containing λDNA. Journal of Applied Polymer Science, **86**, 2557–2566 (2002). https://doi.org/10.1002/app.11178

[15] Díaz E., Valle M. B., Ribeiro S., Lanceros-Mendez S., Barandiarán J. M.: 3D cytocompatible composites of PCL/magnetite. Materials, **12**, 3843 (2019). https://doi.org/10.3390/ma12233843

[16] Bartnikowski M., Dargaville T. R., Ivanovski S., Hutmacher D. W.: Degradation mechanisms of polycaprolactone in the context of chemistry, geometry and environment. Progress in Polymer Science, **96**, 1–20 (2019). https://doi.org/10.1016/j.progpolymsci.2019.05.004

[17] Kumawat V. S., Ghosh S. B., Bandyopadhyay-Ghosh S.: Microporous biocomposite scaffolds with tunable degradation and interconnected microarchitecture-A synergistic integration of bioactive chain silicate glass-ceramic and poly(ε-caprolactone). Polymer Degradation and Stability, **165**, 20–26 (2019). https://doi.org/10.1016/j.polymdegradstab.2019.04.017

[18] Shalchy F., Lovell C., Bhaskar A.: Hierarchical porosity in additively manufactured bioengineering scaffolds: Fabrication & characterisation. Journal of the Mechanical Behavior of Biomedical Materials, **110**, 103968 (2020). https://doi.org/10.1016/j.jmbbm.2020.103968

[19] Chiellini E., Corti A., D'Antone S., Solaro R.: Biodegradation of poly(vinyl alcohol) based materials. Progress in Polymer Science, **28**, 963–1014 (2003). https://doi.org/10.1016/s0079-6700(02)00149-1

[20] Wu Y., Xia H., Zhang B., Zhao Y., Wang Y.: Assessment of polyglycolic acid scaffolds for periodontal ligament regeneration. Biotechnology & Biotechnological Equipment, **32**, 701–706 (2018). https://doi.org/10.1080/13102818.2018.1437358

[21] Zhang J., Yang S., Yang X., Xi Z., Zhao L., Cen L., Lu E., Yang Y.: Novel fabricating process for porous polyglycolic acid scaffolds by melt-foaming using supercritical carbon dioxide. ACS Biomaterials Science and Engineering, **4**, 694–706 (2018). https://doi.org/10.1021/acsbiomaterials.7b00692

[22] Qu X-H., Wu Q., Zhang K-Y., Chen G. Q.: *In vivo* studies of poly(3-hydroxybutyrate-*co*-3-hydroxyhexanoate) based polymers: Biodegradation and tissue reactions. Biomaterials, **27**, 3540–3548 (2006). https://doi.org/10.1016/j.biomaterials.2006.02.015

[23] Kehail A. A., Boominathan V., Fodor K., Chalivendra V., Ferreira T., Brigham C. J.: *In vivo* and i*n vitro* degradation studies for poly(3-hydroxybutyrate-*co*-3-hydroxyhexanoate) biopolymer. Journal of Polymers and the Environment, **25**, 296–307 (2016). https://doi.org/10.1007/s10924-016-0808-1

[24] Kapoor B., Bhattacharya M.: Transient shear and extensional properties of biodegradable polycaprolactone. Polymer Engineering and Science, **39**, 676–687 (1999). https://doi.org/10.1002/pen.11456

[25] Arcos D., Vallet-Regí M.: Substituted hydroxyapatite coatings of bone implants. Journal of Materials Chemistry B, **8**, 1781–1800 (2020). https://doi.org/10.1039/c9tb02710f

[26] Jeong J., Kim J. H., Shim J. H., Hwang N. S., Heo C. Y.: Bioactive calcium phosphate materials and applications in bone regeneration. Biomaterials Research, **23**, 4 (2019). https://doi.org/10.1186/s40824-018-0149-3

[27] Vyas A., Kumawat V. S., Ghosh S. B., Bandyopadhyay-Ghosh S.: Microstructural analysis and bioactive response of selectively engineered glass-ceramics in simulated body fluid. Materials Technology, **36**, 451–459 (2020). https://doi.org/10.1080/10667857.2020.1774208

[28] Beall G. H.: Chain silicate glass-ceramics. Journal of Non-Crystalline Solids, **129**, 163–173 (1991). https://doi.org/10.1016/0022-3093(91)90092-k

[29] Miller C. A., Kokubo T., Reaney I. M., Hatton P. V., James P. F.: Formation of apatite layers on modified canasite glass–ceramics in simulated body fluid. Journal of Biomedical Materials Research, **59**, 473–480 (2001). https://doi.org/10.1002/jbm.10018

[30] Bandyopadhyay-Ghosh S., Reaney I. M., Brook I. M., Hurrell-Gillingham K., Johnson A., Hatton P. V.: *In vitro* biocompatibility of fluorcanasite glass-ceramics for bone tissue repair. Journal of Biomedical Materials Research Part A, **80**, 175–183 (2007). https://doi.org/10.1002/jbm.a.30878

[31] Bandyopadhyay-Ghosh S., Faria P. E. P., Johnson A., Felipucci D. N. B., Reaney I. M., Salata L. A., Brook I. M., Hatton P. V.: Osteoconductivity of modified fluorcanasite glass–ceramics for bone tissue augmentation and repair. Journal of Biomedical Materials Research Part A, **94**, 760–768 (2010). https://doi.org/10.1002/jbm.a.32750

[32] Bandyopadhyay-Ghosh S., Reaney I. M., Johnson A., Hurrell-Gillingham K., Brook I. M., Hatton P. V.: The effect of investment materials on the surface of cast fluorcanasite glasses and glass–ceramics. Journal of Materials Science: Materials in Medicine, **19**, 839–846 (2008).
https://doi.org/10.1007/s10856-007-3207-2

[33] Kanchanarat N., Bandyopadhyay-Ghosh S., Reaney I. M., Brook I. M., Hatton P. V.: Microstructure and mechanical properties of fluorcanasite glass-ceramics for biomedical applications. Journal of Materials Science, **43**, 759–765 (2008).
https://doi.org/10.1007/s10853-007-2180-y

[34] Okada K., Nandi M., Maruyama J., Oka T., Tsujimoto T., Kondoh K., Uyama H.: Fabrication of mesoporous polymer monolith: A template-free approach. Chemical Communications, **47**, 7422–7424 (2011).
https://doi.org/10.1039/c1cc12402a

[35] Sachlos E., Czernuszka J. T.: Making tissue engineering scaffolds work. Review on the application of solid freeform fabrication, technology to the production of tissue engineering scaffolds. European Cells and Materials, **5**, 29–40 (2003).
https://doi.org/10.22203/ecm.v005a03

[36] Peltola S. M., Melchels F. P. W., Grijpma D. W., Kellomäki M.: A review of rapid prototyping techniques for tissue engineering purposes. Annals of Medicine, **40**, 268–280 (2008).
https://doi.org/10.1080/07853890701881788

[37] Hutmacher D. W., Schantz T., Zein I., Ng K. W., Teoh S. H., Tan K. C.: Mechanical properties and cell cultural response of polycaprolactone scaffolds designed and fabricated *via* fused deposition modeling. Journal of Biomedical Materials Research, **55**, 203–216 (2001).
https://doi.org/10.1002/1097-4636(200105)55:2<203::aid-jbm1007>3.0.co;2-7

[38] Yeong W. Y., Chua C-K., Leong K-F., Chandrasekaran M.: Rapid prototyping in tissue engineering: Challenges and potential. Trends in Biotechnology, **22**, 643–652 (2004).
https://doi.org/10.1016/j.tibtech.2004.10.004

[39] Boparai K. S., Singh R., Singh H.: Development of rapid tooling using fused deposition modeling: A review. Rapid Prototyping Journal, **22**, 281–299 (2016).
https://doi.org/10.1108/rpj-04-2014-0048

[40] Kumawat V. S., Vyas A., Bandyopadhyay-Ghosh S., Ghosh S. B.: Selectively modified nanostructured fluorcanasite glass-ceramic with enhanced micromechanical properties. Journal of Non-Crystalline Solids, **547**, 120303 (2020).
https://doi.org/10.1016/j.jnoncrysol.2020.120303

[41] Strawhecker K. E., Manias E.: Structure and properties of poly(vinyl alcohol)/Na^+ montmorillonite nanocomposites. Chemistry of Materials, **12**, 2943–2949 (2000).
https://doi.org/10.1021/cm000506g

[42] Ong C. J., Price F. P.: Blends of poly(ε-caprolactone) with poly(vinyl chloride). I. Morphology. Journal of Polymer Science: Polymer Symposia, **63**, 45–58 (1978).
https://doi.org/10.1002/polc.5070630108

[43] Zhang Y., Leblanc-Boily V., Zhao Y., Prud'homme R. E.: Wide angle X-ray diffraction investigation of crystal orientation in miscible blend of poly(ε-caprolactone)/poly(vinyl chloride) crystallized under strain. Polymer, **46**, 8141–8150 (2005).
https://doi.org/10.1016/j.polymer.2005.06.114

[44] Bittiger H., Marchessault R. H., Niegisch W D.: Crystal structure of poly(ε-caprolactone). Acta Crystallographica Section B, **26**, 1923–1927 (1970).
https://doi.org/10.1107/s0567740870005198

[45] Ravi M., Song S., Wang J., Nadimicherla R., Zhang Z.: Preparation and characterization of biodegradable poly (ε-caprolactone)-based gel polymer electrolyte films. Ionics, **22**, 661–670 (2016).
https://doi.org/10.1007/s11581-015-1586-9

[46] Miller C. A., Reaney I. M., Hatton P. V., James P. F.: Crystallization of canasite/frankamenite-based glass-ceramics. Chemistry of Materials, **16**, 5736–5743 (2004).
https://doi.org/10.1021/cm048946l

[47] Yoon B-H., Kim H-W., Lee S-L., Bae C-J., Koh Y-H., Kong Y-M., Kim H.: Stability and cellular responses to fluorapatite–collagen composites. Biomaterials, **26**, 2957–2963 (2005).
https://doi.org/10.1016/j.biomaterials.2004.07.062

[48] Farag M. M., El-Rashedi A. M. I., Rüssel C.: *In vitro* biocompatibility evaluation of canasite-calcium phosphate glass-ceramics. Journal of Non-Crystalline Solids, **488**, 24–35 (2018).
https://doi.org/10.1016/j.jnoncrysol.2018.03.003

[49] Kim H-W., Lee E-J., Kim H-E., Salih V., Knowles J. C.: Effect of fluoridation of hydroxyapatite in hydroxyapatite-polycaprolactone composites on osteoblast activity. Biomaterials, **26**, 4395–4404 (2005).
https://doi.org/10.1016/j.biomaterials.2004.11.008

[50] Chen H-I., Chen W-S., Huang W-C.: Pre-reaction temperature effect on C–S–H colloidal properties and xonotlite formation via steam assisted crystallization. Materials and Structures, **49**, 905–915 (2015).
https://doi.org/10.1617/s11527-015-0547-0

[51] Baji A., Wong S-C., Liu T., Li T., Srivatsan T. S.: Morphological and X-ray diffraction studies of crystalline hydroxyapatite-reinforced polycaprolactone. Journal of Biomedical Materials Research Part B, **81**, 343–350 (2007).
https://doi.org/10.1002/jbm.b.30671

[52] Liu Y., Yang S., Cao L., Zhang X., Wang J., Liu C.: Facilitated vascularization and enhanced bone regeneration by manipulation hierarchical pore structure of scaffolds. Materials Science and Engineering: C, **110**, 110622 (2020).
https://doi.org/10.1016/j.msec.2019.110622

[53] Liu H., Yazici H., Ergun C., Webster T. J., Bermek H.: An *in vitro* evaluation of the Ca/P ratio for the cytocompatibility of nano-to-micron particulate calcium phosphates for bone regeneration. Acta Biomaterialia, **4**, 1472–1479 (2008). https://doi.org/10.1016/j.actbio.2008.02.025

[54] Lu L., Zhang Q., Wootton D. M., Chiou R., Li D., Lu B., Lelkes P. I., Zhou J.: Mechanical study of polycaprolactone-hydroxyapatite porous scaffolds created by porogen-based solid freeform fabrication method. Journal of Applied Biomaterials & Functional Materials, **12**, 145–154 (2014). https://doi.org/10.5301/jabfm.5000163

[55] da Cunha D. A. L. V., Neto P. I., Micocci K. C., Bellani C. F., Selistre-de-Araujo H. S., Silveira Z. C., Branciforti M. C.: Fabrication and characterization of scaffolds of poly(ε-caprolactone)/Biosilicate® biocomposites prepared by generative manufacturing process. International Journal of Biomaterials, **2019**, 2131467 (2019). https://doi.org/10.1155/2019/2131467

[56] Eshraghi S., Das S.: Mechanical and microstructural properties of polycaprolactone scaffolds with one-dimensional, two-dimensional, and three-dimensional orthogonally oriented porous architectures produced by selective laser sintering. Acta Biomaterialia, **6**, 2467–2476 (2010). https://doi.org/10.1016/j.actbio.2010.02.002

[57] Roohani-Esfahani S. I., Nouri-Khorasani S., Lu Z. F., Appleyard R. C., Zreiqat H.: Effects of bioactive glass nanoparticles on the mechanical and biological behavior of composite coated scaffolds. Acta Biomaterialia, **7**, 1307–1318 (2011). https://doi.org/10.1016/j.actbio.2010.10.015

[58] Nejati E., Firouzdor V., Eslaminejad M. B., Bagheri F.: Needle-like nano hydroxyapatite/poly(L-lactide acid) composite scaffold for bone tissue engineering application. Materials Science and Engineering: C, **29**, 942–949 (2009). https://doi.org/10.1016/j.msec.2008.07.038

[59] Al-Harbi N., Mohammed H., Al-Hadeethi Y., Bakry A. S., Umar A., Hussein M. A., Abbassy M. A., Vaidya K. G., Al Berakdar G., Mkawi E. M., Nune M.: Silica-based bioactive glasses and their applications in hard tissue regeneration: A review. Pharmaceuticals, **14**, 1–20 (2021). https://doi.org/10.3390/ph14020075

[60] Kim J-W., Shin K-H., Koh Y-H., Hah M. J., Moon J., Kim H-E.: Production of poly(ε-caprolactone)/hydroxyapatite composite scaffolds with a tailored macro/micro-porous structure, high mechanical properties, and excellent bioactivity. Materials, **10**, 1123 (2017). https://doi.org/10.3390/ma10101123